DRAFT
CMS Paper

2020/10/20
Archive Hash: 4618801-D
Archive Date: 2020/10/20

~~Differential~~ cross section ~~measurements of the production of~~ Z bosons with charm jets in p~~roton~~ p~~roton~~ collisions at $\sqrt{s} = 13$ TeV

The CMS Collaboration

Abstract

Measurements of differential cross sections of the ~~production of a~~ Z boson in association with at least one jet initiated by a charm quark in p~~roton~~ p~~roton~~ collisions at $\sqrt{s} = 13$ TeV ~~are presented~~. The data ~~were~~ recorded ~~in 2016~~ by the CMS experiment at the LHC ~~and~~ correspond to an integrated luminosity of 35.9 fb^{-1}. The ~~measurements are performed in~~ final states that ~~include~~ a pair of electrons or muons consistent with being the decay products of a Z boson, ~~plus~~ a jet consistent with being initiated by a charm quark produced in the hard interaction. The ~~electrons or muons~~ are ~~both~~ required to have $|\eta| < 2.4$ and $p_T > 10$ GeV, at least one must have $p_T > 30$ GeV, and ~~the invariant~~ mass of the pair ~~must be~~ in the range 71–111 GeV. The c jet ~~candidate~~ is required to have $p_T > 30$ GeV and $|\eta| < 2.4$.

Differential cross sections ~~with respect to the transverse momentum~~ of the Z boson ~~candidate~~ and ~~with respect to the transverse momentum~~ of the charm jet are ~~measured, and~~ compared with predictions from ~~different~~ Monte Carlo generators. The inclusive production cross section in ~~the~~ fiducial region is found to be $405.4 \pm 5.6(\text{stat}) \pm 23.5(\text{exp}) \pm 8.1(\text{th})$ pb. These are the first measurements of this process in p~~roton~~ p~~roton~~ collisions at 13 TeV.

This box is only visible in draft mode. Please make sure the values below make sense.

PDFAuthor:	Anton Stepennov
PDFTitle:	Differential cross section measurements of the production of Z bosons with charm jets in proton-proton collisions at sqrts=13 TeV
PDFSubject:	CMS
PDFKeywords:	CMS, physics, your topics

Please also verify that the abstract does not use any user defined symbols

1 Introduction

The CERN LHC has delivered ~~large samples of~~ $\sqrt{s} = 13\,\text{TeV}$ ~~proton-proton (~~pp~~)~~ collision ~~events~~ ~~in which~~ a Z boson ~~is~~ accompanied by one or more jets initiated by charm quarks (c jets). ~~Measurements of the~~ differential cross section~~s~~ ~~of~~ inclusive Z+c jet production ~~with respect to~~ the transverse momenta p_{T} of the Z boson and c jet can ~~test existing theoretical~~ models, provide information on the ~~charm quark~~ parton distribution function (PDF), and ~~test~~ the possibility of observing the intrinsic charm quark (IC) component in the nucleon [1–3]. An IC component would enhance the rate of Z+c jet production, ~~in particular~~ at large values of ~~the transverse momentum~~ of the Z boson and of the c jet.

Associated production of a Z boson and a c jet is ~~also~~ an important background in searches for physics beyond the ~~St~~andard ~~M~~odel (SM). For example, in supersymmetry ~~models~~ a top squark ($\tilde{\text{t}}$) can decay into a charm quark and an undetected lightest supersymmetric particle (LSP), ~~leaving~~ a large p_{T} imbalance [4]. One of the backgrounds for such a process is Z+c jet production with the Z boson decaying into neutrinos. Improving the modelling of Z+c jet production ~~by studying~~ visible decay modes ~~will~~ therefore enhance this and similar searches. An example of a Feynman diagram corresponding to the Z+c jet process, sensitive to the charm quark PDF, is shown in Fig. 1.

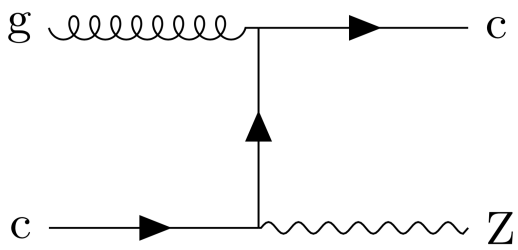

Figure 1: Example Feynman diagram for the Z+c jet process.

~~Previous~~ measurement of Z+c jet cross section at 8 TeV can be found in [5]. Here we present a study of events containing a candidate Z boson and a candidate c jet. The Z boson candidate is formed from an identified electron or muon pair, and the c jet candidate is identified by applying charm tagging criteria [6] to ~~the~~ reconstructed jets.

~~In order to allow~~ direct comparison with predictions from ~~different theoretical~~ models at the level of Monte Carlo (MC) event ~~generator output~~ (generator level), we unfold detector effects from our measurements. The data ~~used~~, corresponding to an integrated luminosity of 35.9 fb^{-1} at $\sqrt{s} = 13\,\text{TeV}$, were recorded by the CMS experiment during pp collisions ~~in 2016~~.

~~The m~~easurements of the differential cross sections of Z+c jet production as a function of the p_{T} of the Z boson ~~candidate~~ and as a function of the c-tagged jet p_{T} are performed in several steps. The first step is to select c jet-enriched samples of $\text{Z} \to \text{ee}$ (electron channel) or $\text{Z} \to \mu\mu$ (muon channel) candidate events. The second step is to split the sample into different bins according to the p_{T} of the Z boson ~~candidate~~ or c-tagged jet, and ~~to~~ measure the number of Z+c jet events in each bin. The third step is to unfold the data, using the simulation of the signal to ~~build~~ response matrices to relate the observed distributions to the generator level. The final step is to combine the resulting unfolded electron and muon channel p_{T} distributions, and ~~to~~ compare them with predictions from different MC event generators.

2 The CMS detector

The central feature of the CMS apparatus is a superconducting solenoid of 6 m internal diameter, providing a magnetic field of 3.8 T. ~~Within the solenoid volume are a~~ silicon pixel and strip tracker, covering a pseudorapidity region $|\eta| < 2.5$, a lead tungstate crystal electromagnetic calorimeter (ECAL), and a brass and scintillator hadron calorimeter~~. Each of these systems is~~ composed of a barrel and two end~~cap~~ sections~~.~~ Forward calorimeters, made of steel and quartz fibers, extend η coverage provided by the barrel and endcap detectors to $|\eta| < 5$. Muons are detected in gas-ionization chambers embedded in the steel flux-return yoke outside the solenoid ~~and~~ cover~~ing~~ $|\eta| < 2.4$. Events of interest are selected using a two-tiered trigger system [7]. The first level, composed of ~~custom~~ hardware processors, uses information from the calorimeters and muon detectors to select events at a rate of ~~around~~ 100 kHz within a fixed time interval of about 4 μs. The second level, known as the high-level trigger, consists of a farm of processors running a version of the full event reconstruction software optimized for fast processing~~, and~~ reduces the event rate to ~~around~~ 1 kHz before data storage. A more detailed description of the CMS detector, together with a definition of the coordinate system ~~used~~ and ~~the relevant~~ kinematic variables, can be found in Ref. [8].

3 Data and simulated ~~samples~~

The measurements of the cross section are based on 35.9 fb^{-1} pp collision data collected by the CMS detector ~~in 2016~~. The minimum proton bunch spacing is 25 ns with 23 additional interactions (pileup) on average per beam crossing.

Different MC generators are used to simulate Z+jets background and signal processes. The MADGRAPH5_aMC@NLO version 2.2.2 [9] (MG5_aMC) generator is used to simulate Drell–Yan (DY) processes, including the Z+c jet signal, calculated at next-to-leading order (NLO). Background DY events include those with a Z boson and a jet initiated by a bottom quark (b jet), or a jet initiated by a light quark or a gluon (light jet). Samples are made for Z+n jet processes ($n \leq 2$), calculated at NLO in perturbative QCD. A second signal model is provided by using MG5_aMC to calculate leading order (LO) matrix elements for $\text{pp} \to \text{Z} + n$ jets ($n \leq 4$). For a third signal model, SHERPA v2.2 [10, 11] is used to generate $\text{pp} \to \text{Z} + n$ jets events, with $n \leq 2$ at NLO and $n \leq 4$ at LO. All three signal models are normalized to the value of the inclusive Z + jets cross section calculated at next-to-next-to-leading order with FEWZ v3.1 [12]. These samples are generated using the NNPDF 3.0 [13] PDF set.

As well as events with light and b jets, there is a contribution to the background from processes producing top quark pairs [14, 15] and single top quarks [16, 17]. These samples were generated using NLO POWHEG v2.0 [18–20] or MG5_aMC. There is also background from vector boson pair production, which is simulated using PYTHIA 8 v8.212 [21].

All samples, except SHERPA, use PYTHIA 8 to model the initial- and final-state parton showers and hadronization, with the CUETP8M1 [22] or CUETP8M2T4 [23] (top pair sample) tune that includes the NNPDF 2.3 [24] LO PDFs and the value of the strong coupling at the mass of the Z boson set as $\alpha_S(m_Z) = 0.119$. Matching between the matrix element generators and the parton shower is done using the k_T–MLM [25, 26] scheme with the matching scale set at 19 GeV for the LO MG5_aMC samples, and the FxFx [27] scheme with the matching scale set to 30 GeV for the NLO MG5_aMC ~~samples~~.

GEANT4 [28] is used for CMS detector simulation. The simulation takes account of additional pp interactions (pileup) in the current and nearby bunch crossing.

4 Object reconstruction and event selection

The particle flow (PF) algorithm [29] is used to reconstruct and identify individual particle candidates in an event, ~~with~~ an optimized combination of information from the various elements of the CMS detector. Energy deposits are measured in the calorimeters, while charged particles are identified in the central tracking and muon systems.

Electrons are reconstructed from tracks, fitted with a Gaussian sum filter, matching energy deposits in the ECAL [30]. Identification requirements based on the ECAL shower shape, matching between the track and the ECAL deposits, and observables characterizing the emission of bremsstrahlung radiation along the electron trajectory are applied. Electrons are required to originate from the primary vertex, which is the vertex candidate with the largest value of summed physics-object p_T^2. Longitudinal and transverse impact parameters for barrel (endcap) are required to be $<$0.10 (0.20) and 0.05 (0.10) cm, respectively. The electron momentum is estimated by combining the energy measurement in the ECAL with the momentum measurement in the tracker. The momentum resolution for electrons with $p_T \approx 45\,\text{GeV}$ from $Z \to ee$ decays ranges from 1.7% to 4.5%. The dielectron mass resolution for $Z \to ee$ decays when both electrons are in the ECAL barrel is 1.9%, degrading to 2.9% when both electrons are in the endcaps.

Muons are reconstructed by combining signals from the inner tracker and the muon detector subsystems. They are required to satisfy standard identification criteria based on the number of hits in each detector, the track fit quality, and the consistency with the primary vertex by requiring the longitudinal and transverse impact parameters to be $<$0.5 and 0.2 cm, respectively. The efficiency to reconstruct and identify muons is greater than 96% [31]. Matching muons to tracks measured in the silicon tracker results in a relative p_T resolution for muons with $20 < p_T < 100\,\text{GeV}$ of 1% in the barrel and 3% in the ~~end~~caps. In order to reduce the misidentification rate, muons are required to be isolated. The isolation of muons is defined as the sum of the p_T of all additional PF candidates within a cone of radius $\Delta R = \sqrt{(\Delta\eta)^2 + (\Delta\phi)^2} = 0.4$ around the muon track, where ϕ is the azimuthal angle in radians. After compensating for the contribution from pileup [32], the resultant sum is required to be less than 25% of the muon p_T.

Jets are clustered from PF candidates using the infrared- and collinear-safe anti-k_T algorithm with a distance parameter of 0.4, as implemented in the FastJet package [33, 34]. The jet momentum is determined as the vectorial sum of all particle momenta in the jet, and is found from simulation to be within 5 to 10% of the true momentum over the entire p_T spectrum and detector acceptance. To mitigate the effects of pileup, charged particle candidates identified as originating from pileup vertices are discarded and a correction [35] is applied to remove remaining contributions. The reconstructed jet energy scale (JES) is corrected using a factorized model to compensate for the nonlinear and nonuniform response in the calorimeters. Corrections are derived from simulation to bring the measured response of jets to that of generator-level jets on average. In situ measurements of the momentum balance in dijet, multijet, photon+jet, and leptonically decaying Z+jet events are used to account for any residual differences between the JES in data and simulation [36]. The jet energy in simulation is degraded to match the resolution observed in data. The jet energy resolution (JER) amounts typically to 15% at 10 GeV, 8% at 100 GeV, and 4% at 1 TeV. Additional selection criteria are applied to remove jets potentially dominated by anomalous contributions from various subdetector components or reconstruction failures [37]. Jets identified as likely coming from pileup [38] are also removed.

Events are selected online ~~with~~ a single electron trigger requiring at least one electron candidate with $p_T > 27\,\text{GeV}$ (electron channel), or a single muon trigger requiring at least one muon candidate with $p_T > 24\,\text{GeV}$ (muon channel). Offline, we require a pair of ~~opposite-sign~~ electrons

or muons satisfying identification and isolation criteria, with $p_T > 10\,\text{GeV}$ and $|\eta| < 2.4$, and with an invariant mass close to the mass of the Z boson: $71\,\text{GeV} < m_{ee/\mu\mu} < 111\,\text{GeV}$. In the electron channel at least one electron must have $p_T > 29\,\text{GeV}$ and in the muon channel at least one muon must have $p_T > 26\,\text{GeV}$, in order to exceed the trigger thresholds. Small residual differences in the trigger, identification, and isolation efficiencies between data and simulation are measured using "tag-and-probe" methods [39], and taken into account by applying scale factors to simulated events.

The event must contain at least one jet with $p_T > 30\,\text{GeV}$ and $|\eta| < 2.4$, satisfying tight c tagging criteria using the deep combined secondary vertices algorithm [6]. This algorithm allows the discrimination of c jets from b and light jets, based on jet properties such as the presence of secondary vertices and tracks with large impact parameter. Data from W+jets, $t\bar{t}$, and inclusive jet production are used to measure the c tagging efficiency for c jets, and mistag rates for b and light jets. These are compared to the simulation, where the reconstructed jet flavor is known from its hadron content. Small differences between data and simulation are taken into account by applying scale factors to the simulation. The threshold applied in this analysis gives a c tagging efficiency of about 30%, and misidentification probabilities of 1.2% for light jets and 20% for b jets, with relative uncertainties between 5% and 15% depending on the p_T of the jet. If several c-tagged jets are found in the event, the one with the highest p_T is used.

The simulated events are classified according to generator-level information. Generator-level jets are made by clustering all stable particles resulting from hadronization using the anti-k_T algorithm with a distance parameter of 0.4, and the jet flavor is defined by the flavor of the hadrons within the jet. If an event contains a generator-level jet with $p_T > 10\,\text{GeV}$ containing a b hadron, the event is defined as a Z+b jet event. If there is no such generator-level b jet in the event and there is at least one generator-level jet with $p_T > 10\,\text{GeV}$ containing a c hadron, the event is defined as a Z+c jet event. Other events in the DY sample are classified as Z+light jet events. The generator-level leptons are dressed by adding the momenta of all photons within $\Delta R = 0.1$ around the lepton directions.

5 Signal determination and data unfolding

Charm hadrons ~~will~~ decay at ~~a point that is~~ displaced ~~from~~ the primary vertex. This secondary vertex is reconstructed using the inclusive vertex finder algorithm [40]. The invariant mass of tracks associated with the secondary vertex (M_{SV}) in the c-tagged jet [6] can be used to discriminate between signal and background. Figure 2 shows the observed distributions of M_{SV} in the electron and muon channels, compared to the different signal and background contributions predicted by the simulation. Although M_{SV} is an ingredient in the c tagging algorithm, it can be seen that there are sufficient differences remaining in the distributions for the c-tagged samples to provide information on the flavor composition.

The top quark and diboson background predictions are taken directly from simulation. The normalizations for the Z+c jet, Z+b jet and Z+light jet components are then obtained by fitting templates of the M_{SV} distribution obtained from simulation to the observed data. A maximum likelihood template fit is performed separately in each bin of Z boson candidate or c-tagged jet p_T.

The values of the scale factor SF_q, defined as the ratio of the fitted normalization to the prediction from simulation, are presented in Tables 1–4 for each p_T bin for each Z+q jet process. Sources of systematic uncertainty are discussed in Sec. 6. Figure 3 shows the distributions of the Z boson candidate and c-tagged jet p_T after applying these scale factors, assuming they

are constant across the p_T range in which they are determined. Good agreement is observed between simulation and data after applying these factors.

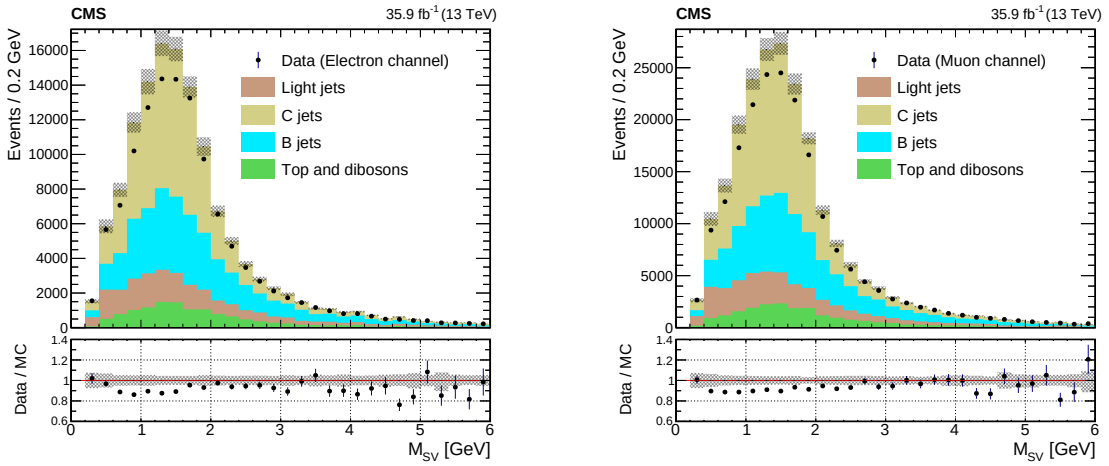

Figure 2: Distribution of the secondary vertex mass of the highest-p_T c-tagged central jet, for electron (left) and muon (right) channels.The observed data is compared to the different signal and background components in simulation, before normalization scale factors are applied.

Table 1: Values of Z+light jet, Z+c jet, and Z+b jet scale factors measured in the electron channel, as a function of c-tagged jet p_T. The first uncertainty in each case is the statistical uncertainty from the fit, the second is the systematic uncertainty.

c-tagged jet p_T (GeV)	SF_l	SF_c	SF_b
30 - 37	$1.16 \pm 0.05\ ^{+0.29}_{-0.21}$	$0.70 \pm 0.04\ ^{+0.09}_{-0.11}$	$1.06 \pm 0.05\ ^{+0.16}_{-0.12}$
37 - 45	$0.79 \pm 0.06\ ^{+0.26}_{-0.18}$	$0.89 \pm 0.03\ ^{+0.10}_{-0.08}$	$0.92 \pm 0.05\ ^{+0.16}_{-0.16}$
45 - 60	$0.97 \pm 0.06\ ^{+0.23}_{-0.19}$	$0.74 \pm 0.03\ ^{+0.08}_{-0.06}$	$1.07 \pm 0.06\ ^{+0.09}_{-0.09}$
60 - 90	$0.99 \pm 0.07\ ^{+0.24}_{-0.18}$	$0.87 \pm 0.04\ ^{+0.08}_{-0.08}$	$0.95 \pm 0.07\ ^{+0.09}_{-0.12}$
90 - 250	$0.92 \pm 0.07\ ^{+0.27}_{-0.19}$	$0.98 \pm 0.05\ ^{+0.11}_{-0.10}$	$1.04 \pm 0.07\ ^{+0.08}_{-0.08}$

The generator-level signal is defined to be Z+c jet events with two ~~opposite sign~~ generator-level electrons or muons with $p_T > 10\,\text{GeV}$ (at least one with $p_T > 26\,\text{GeV}$), $|\eta| < 2.4$, and an invariant mass $71 < m_{ee/\mu\mu} < 111\,\text{GeV}$. There must also be at least one generator-level c jet with $p_T > 30\,\text{GeV}$ and $|\eta| < 2.4$. To avoid double counting, jets within $\Delta R = 0.4$ of one of the two leptons from the Z candidate are removed.

A fraction of Z+c jet events that are outside the signal phase space will migrate into the reconstructed signal region, primarily events with c jets with generated $p_T < 30\,\text{GeV}$ but reconstructed $p_T > 30\,\text{GeV}$ due to the finite detector resolution. The fraction of Z+c jet events that are inside the signal phase space is estimated from the number of selected events in which the c-tagged jet and lepton pair match within $\Delta R < 0.3$ to a generator-level highest p_T c jet and lepton pair satisfying the phase space requirements. Figure 4 shows this fraction as a function of Z boson and c-tagged jet p_T, for electron and muon channels, calculated using MADGRAPH5_aMC@NLO ~~sample~~.

Response matrices are constructed using the Z+c jet events in the DY sample simulated using the MG5_aMC (NLO) generator, and cross-checked using the MG5_aMC (LO) generator. Each

Table 2: Values of Z+light jet, Z+c jet, and Z+b jet scale factors measured in the electron channel, as a function of Z candidate p_{T}. The first uncertainty in each case is the statistical uncertainty from the fit, the second is the systematic uncertainty.

Z candidate p_{T} (GeV)	SF_l	SF_c	SF_b
0 - 30	$0.86 \pm 0.05\ ^{+0.24}_{-0.18}$	$0.76 \pm 0.04\ ^{+0.11}_{-0.09}$	$1.25 \pm 0.07\ ^{+0.17}_{-0.18}$
30 - 50	$0.98 \pm 0.05\ ^{+0.23}_{-0.17}$	$0.80 \pm 0.03\ ^{+0.08}_{-0.08}$	$0.91 \pm 0.05\ ^{+0.10}_{-0.08}$
50 - 65	$0.85 \pm 0.07\ ^{+0.21}_{-0.16}$	$0.78 \pm 0.04\ ^{+0.15}_{-0.11}$	$1.04 \pm 0.06\ ^{+0.17}_{-0.17}$
65 - 95	$1.14 \pm 0.08\ ^{+0.30}_{-0.22}$	$0.97 \pm 0.04\ ^{+0.08}_{-0.07}$	$0.76 \pm 0.06\ ^{+0.09}_{-0.11}$
95 - 300	$1.01 \pm 0.07\ ^{+0.26}_{-0.20}$	$0.83 \pm 0.05\ ^{+0.07}_{-0.07}$	$1.13 \pm 0.07\ ^{+0.08}_{-0.08}$

Table 3: Values of Z+light jet, Z+c jet, and Z+b jet scale factors measured in the muon channel, as a function of c-tagged jet p_{T}. The first uncertainty in each case is the statistical uncertainty from the fit, the second is the systematic uncertainty.

c-tagged jet p_{T} (GeV)	SF_l	SF_c	SF_b
30 - 37	$0.95 \pm 0.04\ ^{+0.24}_{-0.17}$	$0.82 \pm 0.03\ ^{+0.12}_{-0.07}$	$1.04 \pm 0.05\ ^{+0.11}_{-0.19}$
37 - 45	$0.93 \pm 0.05\ ^{+0.26}_{-0.23}$	$0.82 \pm 0.03\ ^{+0.06}_{-0.06}$	$0.96 \pm 0.05\ ^{+0.12}_{-0.09}$
45 - 60	$0.81 \pm 0.04\ ^{+0.20}_{-0.15}$	$0.79 \pm 0.03\ ^{+0.09}_{-0.06}$	$1.10 \pm 0.04\ ^{+0.08}_{-0.07}$
60 - 90	$0.88 \pm 0.04\ ^{+0.23}_{-0.17}$	$0.80 \pm 0.03\ ^{+0.06}_{-0.08}$	$1.25 \pm 0.05\ ^{+0.12}_{-0.10}$
90 - 250	$0.92 \pm 0.05\ ^{+0.24}_{-0.17}$	$0.79 \pm 0.04\ ^{+0.07}_{-0.06}$	$1.16 \pm 0.06\ ^{+0.12}_{-0.12}$

matrix entry represents the probability for an event generated in the signal phase space within a certain c jet (or Z boson) p_{T} range to end up within a certain reconstructed c jet (or Z boson candidate) p_{T} range. The unfolding was done with 5 detector-level p_{T} bins and 4 generator-level p_{T} bins. The TUNFOLD package v17.5 [41], which is based on a least-squares fit, is then used to invert the response matrices and unfold the distribution of the measured number of Z+c jet events.

Figure 5 shows the efficiency (defined as the fraction of signal events generated in the fiducial phase space that pass all selection criteria after reconstruction) as a function of the generator-level Z boson or c jet p_{T} for electron and muon channels, calculated using the MG5_aMC (NLO) sample. The dominant losses are due to the c tagging and lepton selection efficiencies.

6 Systematic uncertainties

The systematic uncertainties are estimated by varying input parameters and then repeating the unfolding procedure, recalculating the values of the efficiency, response matrix, and number of Z+c jet and background events in each case. The differences observed between the unfolded distributions are taken as the uncertainties. The following uncertainties are included:

- **QCD renormalization scale:** The ambiguity in the choice of QCD renormalization scale (μ_R) and factorization scale (μ_F) leads to uncertainty in theoretical predictions for the DY process. This uncertainty is estimated by ~~varying~~ the values of μ_R and μ_F by factors of 0.5 and 2 relative to the default values, $\mu_F = \mu_R = m_Z$, excluding the $(0.5\mu_F, 2\mu_R)$ and $(0.5\mu_R, 2\mu_F)$ combinations.
- **PDF:** The unfolding is performed with different PDF replicas and compared to the nominal distribution.

Table 4: Values of Z+light jet, Z+c jet, and Z+b jet scale factors measured in the muon channel, as a function of Z candidate p_T. The first uncertainty in each case is the statistical uncertainty from the fit, the second is the systematic uncertainty.

Z candidate p_T (GeV)	SF_l	SF_c	SF_b
0 - 30	$0.97 \pm 0.04\ ^{+0.24}_{-0.20}$	$0.82 \pm 0.03\ ^{+0.09}_{-0.08}$	$1.09 \pm 0.05\ ^{+0.11}_{-0.10}$
30 - 50	$0.91 \pm 0.04\ ^{+0.21}_{-0.16}$	$0.80 \pm 0.02\ ^{+0.07}_{-0.06}$	$0.99 \pm 0.04\ ^{+0.05}_{-0.06}$
50 - 65	$0.63 \pm 0.06\ ^{+0.17}_{-0.13}$	$0.73 \pm 0.03\ ^{+0.09}_{-0.06}$	$1.24 \pm 0.05\ ^{+0.09}_{-0.10}$
65 - 95	$0.96 \pm 0.05\ ^{+0.25}_{-0.18}$	$0.85 \pm 0.03\ ^{+0.09}_{-0.06}$	$1.04 \pm 0.05\ ^{+0.13}_{-0.14}$
95 - 300	$0.89 \pm 0.05\ ^{+0.23}_{-0.17}$	$0.78 \pm 0.04\ ^{+0.07}_{-0.07}$	$1.33 \pm 0.06\ ^{+0.08}_{-0.08}$

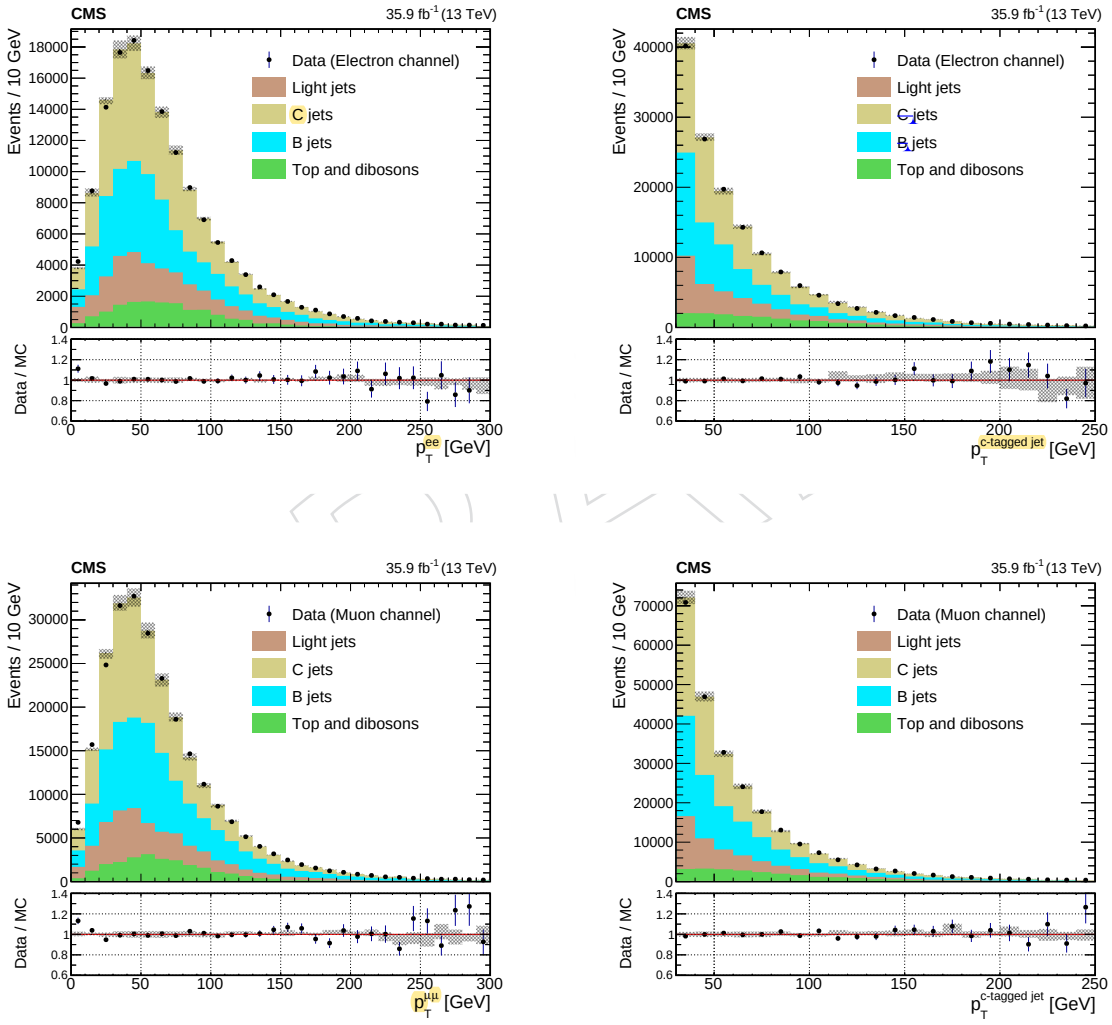

Figure 3: The distributions of p_T in data and corrected simulation, after applying the fitted scale factors to the Drell-Yan components. The upper plots show distributions for the electron channel, with the p_T of the electron pair (left) and c-tagged jet (right). The lower plots show distributions for the muon channel with the p_T of the muon pair (left) and c-tagged jet (right).

- **c tagging efficiency:** The effect of uncertainties in the c tagging rates is estimated

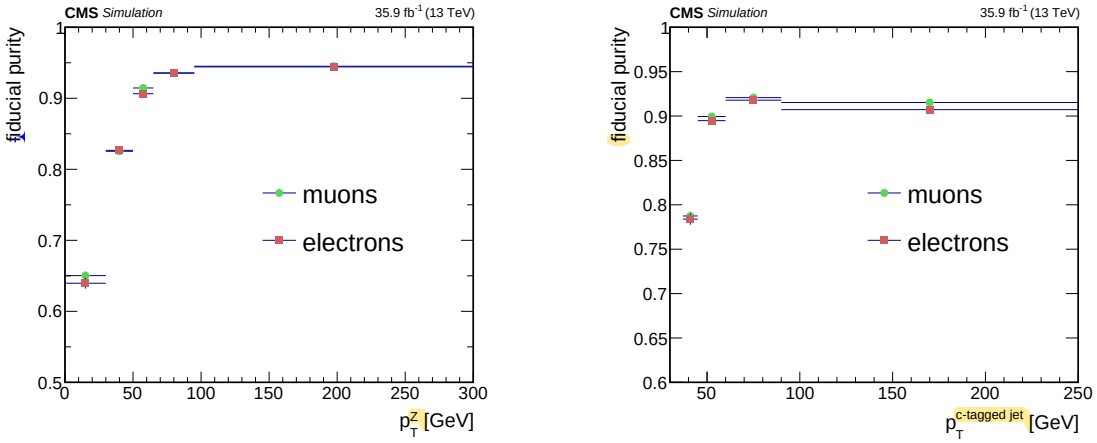

Figure 4: Fraction of selected Z+c jet events originating ~~inside~~ the fiducial phase space~~,~~ as a function of p_{T}. Plots show distributions for electron and muons~~-~~ channels, as a function of ~~p_{T} of the Z candidate (left)~~ and ~~c tagged jet (right)~~.

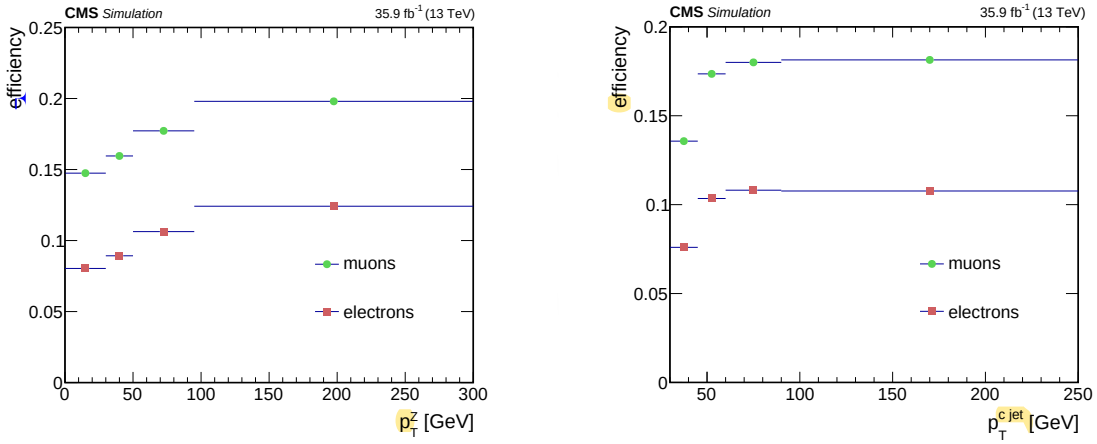

Figure 5: Efficiency as a function of p_{T}. The plots show distributions for the electron and muon channels, as a function of ~~p_{T} of the Z boson (left)~~ and ~~c jet (right)~~.

by varying tagging and mistagging scale factors for the different jet flavors. Scale factors for tagging c jets, and mistagging b jets and light jets are varied up and down by one standard deviation. The combined c tagging uncertainty is then calculated as the sum in quadrature of these variations. The variation of scale factors is $\sim$ 15% for light jets, and ~~$\sim$~~ 5% for charm and bottom jets.

- **Jet energy resolution and scale:** Both the JES and JER corrections can affect jet p_{T} and the secondary vertex mass distributions used in the SF_b and SF_l measurements. The uncertainty resulting from JES corrections is estimated by varying the p_{T}- and η-dependent scale factors within their uncertainty (up to $\sim$ 4%). The JER uncertainty is estimated by varying the amount of jet p_{T} resolution degradation applied to the simulation up and down by one standard deviation ($\sim$ 10%).

- **Pileup:** The corresponding uncertainty is estimated by ~~varying~~ the total inelastic cross section by $\pm 4.6\%$ [42].
- **Lepton identification and isolation:** Uncertainties resulting from the modeling of the identification and isolation of muons and electrons are estimated by varying the corresponding scale factors within their uncertainties. For electrons the uncertainty is less than 3%, while for muons uncertainties in identification and isolation are less than 2%.
- **Top pair production cross section:** The uncertainty due to the cross section used for the modeling of top quark pair production is taken into account by varying the normalization of the top pair component of the background by $\pm 10\%$ [43].
- **Luminosity:** The uncertainty is obtained by varying the luminosity value used to normalize the unfolded distributions by $\pm 2.5\%$ [44]
- **Statistical uncertainties of M_{SV} templates:** The uncertainty is obtained by taking into account statistical fluctuations in each bin of the simulated M_{SV} distributions, used in the fit of SF_l, SF_c and SF_b.

Table 5 summarizes the uncertainties on the inclusive fiducial cross section due to the different sources considered.

Table 5: Summary of the systematic uncertainties on the integral fiducial cross section arising from the various sources considered.

Channel	QCD (%)	PDF (%)	c tag/mistag (%)	JER (%)	JES (%)	Pileup (%)	Top Pair (%)	ID\Iso (%)	$\mathcal{L}$ (%)	MC stat. (%)
$\mu\mu, p_T(\text{c jet})$	5.4	0.5	4.3	4.2	5.7	1.4	0.6	1.0	2.5	1.4
	-5.4	-0.4	-4.0	-3.7	-4.0	-1.6	-0.6	-1.0	-2.5	-1.4
$\mu\mu, p_T(\text{Z})$	2.2	0.6	4.4	1.2	3.9	1.5	0.9	1.0	2.5	1.8
	-1.5	-0.5	-4.1	-1.1	-3.9	-1.9	-0.7	-1.0	-2.5	-1.8
ee, $p_T(\text{c jet})$	6.2	0.6	4.1	3.2	5.6	2.8	0.3	2.4	2.5	1.8
	-5.9	-0.7	-4.1	-4.0	-7.5	-3.3	-0.7	-2.8	-2.5	-1.8
ee, $p_T(\text{Z})$	2.8	0.6	4.4	1.1	5.3	1.8	0.7	2.6	2.5	2.0
	-2.0	-0.6	-4.0	-1.0	-4.3	-1.8	-0.6	-2.6	-2.5	-2.0

7 Results

The differential cross sections are obtained from the unfolded distributions as

$$\frac{d\sigma}{dp_T} = \frac{N_i}{\mathcal{L}\Delta_i \mathcal{B}(Z \to \ell\ell)}, \tag{1}$$

where N_i is the number of events in p_T bin i of the unfolded distribution, Δ_i is the width of the bin, $\mathcal{L}$ is the integrated luminosity, and $\mathcal{B}(Z \to \ell\ell) = 3.36\%$ is the branching fraction of the Z boson to $\ell\ell$ with $\ell = e$ or μ.

The total fiducial cross section is measured as

$$\sigma_{fid} = \frac{N_{charm} P_{fid}}{\varepsilon \mathcal{L} \mathcal{B}(Z \to \ell\ell)}, \tag{2}$$

where N_{charm} is the integral number of measured charm events, P_{fid} is the integral fiducial purity and ε is the integral fiducial selection efficiency.

The results of the measurements of differential and fiducial cross sections from the electron and muon channels are combined by a fit using the CONVINO tool [45], taking into account statistical and systematic uncertainties. The uncertainties relating to the c tag/mistag rates, JER, JES,

pileup, luminosity, and top quark pair cross section are taken as fully correlated between the channels, while uncertainties from other sources are assumed to be uncorrelated. The experimental systematic uncertainties are those related to c tag/mistag rates, JER, JES, identification and isolation, pileup, and luminosity. The rest are designated as theoretical systematic uncertainties. The values of the cross sections as a function of p_{T} of the Z boson and c jet after combining are shown in Fig. 6. This also shows a comparison of the measured fiducial cross sections with predictions from the generators MG5_aMC (NLO), MG5_aMC (LO), and SHERPA. The inclusive fiducial cross section value for Z boson $p_{\mathrm{T}} < 300\,\mathrm{GeV}$ equals $405.4 \pm 5.6(\mathrm{stat}) \pm 23.5(\mathrm{exp}) \pm 8.1(\mathrm{th})$ pb, where (exp) and (th) denote experimental and theoretical systematic uncertainties respectively. This value is significantly lower than the MG5_aMC (NLO) predicted value of $524.9 \pm 11.7(\mathrm{th})$ pb. The experimental systematic uncertainty includes QCD scale and PDF ~~uncertainties~~.

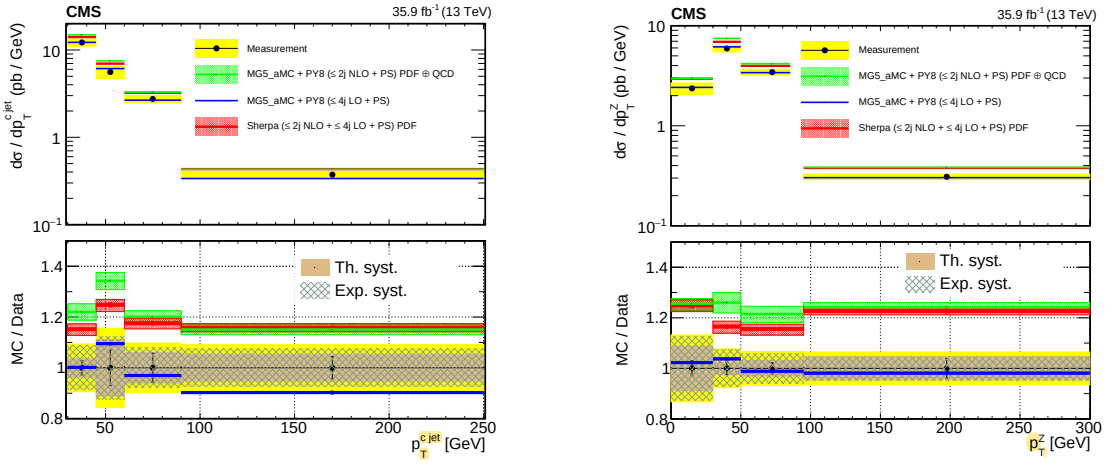

Figure 6: Measured fiducial differential cross sections for inclusive Z+c jet production, $\frac{d\sigma}{dp_{\mathrm{T}}(\mathrm{c\ jet})}$ (left) and $\frac{d\sigma}{dp_{\mathrm{T}}(\mathrm{Z})}$ (right).

8 Summary

The first differential cross sections ~~measurement~~ for inclusive Z+c jet production ~~with respect to the~~ transverse momentum p_T of the Z boson and ~~the~~ c jet ~~have been made in proton-proton~~ collisions at $\sqrt{s} = 13\,\text{TeV}$ ~~using~~ $35.9\,\text{fb}^{-1}$ of data collected by the CMS experiment at the LHC. The measurements pertain to a fiducial space defined as containing a c jet with $p_T > 30\,\text{GeV}$ and pseudorapidity $|\eta| < 2.4$, and a pair of leptons with $p_T > 10\,\text{GeV}$ (at least one with $p_T > 26\,\text{GeV}$~~,~~), $|\eta| < 2.4$, and ~~an invariant~~ mass between 71 and 111 GeV. The main backgrounds ~~considered were~~ Z+light jet, Z+b jet, ~~top pair,~~ and diboson production. ~~Unfolding was used~~ to ~~take into~~ account detector ~~effects~~.

The inclusive fiducial cross section ~~value~~ for the ~~signal process with~~ Z boson $p_T < 300\,\text{GeV}$ ~~was~~ found to be $405.4 \pm 5.6(\text{stat}) \pm 23.5(\text{exp}) \pm 8.1(\text{th})$ pb, while the MADGRAPH5_aMC@NLO generator at next-to-leading order predicts $524.9 \pm 11.7(\text{th})$ pb for the same fiducial region. The ~~theoretical~~ systematic uncertainty includes QCD ~~scale~~ and ~~PDF uncertainties~~. The predictions from ~~several~~ MC generators were compared with measurements~~. The prediction from~~ MADGRAPH5_aMC@NLO at leading order ~~shows good agreement with data~~, while both MADGRAPH5_aMC@NLO and SHERPA at next-to-leading order tend to overestimate the cross section ~~value~~. Predictions from all three generators were normalized to the cross section calculated with FEWZ at next-to-next-to-leading order. Since the prediction of inclusive Z+jets production at next-to-leading order is in ~~better~~ agreement with data than that at leading order [46], this could be an indication that the parton distribution functions overestimate the charm content. These results can improve ~~the~~ existing constraints on the ~~parton distribution function~~ of the charm quark.

Acknowledgments

We congratulate our colleagues in the CERN accelerator departments for the excellent performance of the LHC and thank the technical and administrative staffs at CERN and at other CMS institutes for their contributions to the success of the CMS effort. In addition, we gratefully acknowledge the computing centers and personnel of the Worldwide LHC Computing Grid for delivering so effectively the computing infrastructure essential to our analyses. Finally, we acknowledge the enduring support for the construction and operation of the LHC and the CMS detector provided by the following funding agencies: BMBWF and FWF (Austria); FNRS and FWO (Belgium); CNPq, CAPES, FAPERJ, FAPERGS, and FAPESP (Brazil); MES (Bulgaria); CERN; CAS, MoST, and NSFC (China); COLCIENCIAS (Colombia); MSES and CSF (Croatia); RPF (Cyprus); SENESCYT (Ecuador); MoER, ERC IUT, PUT and ERDF (Estonia); Academy of Finland, MEC, and HIP (Finland); CEA and CNRS/IN2P3 (France); BMBF, DFG, and HGF (Germany); GSRT (Greece); NKFIA (Hungary); DAE and DST (India); IPM (Iran); SFI (Ireland); INFN (Italy); MSIP and NRF (Republic of Korea); MES (Latvia); LAS (Lithuania); MOE and UM (Malaysia); BUAP, CINVESTAV, CONACYT, LNS, SEP, and UASLP-FAI (Mexico); MOS (Montenegro); MBIE (New Zealand); PAEC (Pakistan); MSHE and NSC (Poland); FCT (Portugal); JINR (Dubna); MON, RosAtom, RAS, RFBR, and NRC KI (Russia); MESTD (Serbia); SEIDI, CPAN, PCTI, and FEDER (Spain); MOSTR (Sri Lanka); Swiss Funding Agencies (Switzerland); MST (Taipei); ThEPCenter, IPST, STAR, and NSTDA (Thailand); TUBITAK and TAEK (Turkey); NASU (Ukraine); STFC (United Kingdom); DOE and NSF (USA).

Individuals have received support from the Marie-Curie program and the European Research Council and Horizon 2020 Grant, contract Nos. 675440, 752730, and 765710 (European Union); the Leventis Foundation; the A.P. Sloan Foundation; the Alexander von Humboldt Founda-

tion; the Belgian Federal Science Policy Office; the Fonds pour la Formation à la Recherche dans l'Industrie et dans l'Agriculture (FRIA-Belgium); the Agentschap voor Innovatie door Wetenschap en Technologie (IWT-Belgium); the F.R.S.-FNRS and FWO (Belgium) under the "Excellence of Science – EOS" – be.h project n. 30820817; the Beijing Municipal Science & Technology Commission, No. Z191100007219010; the Ministry of Education, Youth and Sports (MEYS) of the Czech Republic; the Deutsche Forschungsgemeinschaft (DFG) under Germanys Excellence Strategy – EXC 2121 "Quantum Universe" – 390833306; the Lendület ("Momentum") Program and the János Bolyai Research Scholarship of the Hungarian Academy of Sciences, the New National Excellence Program ÚNKP, the NKFIA research grants 123842, 123959, 124845, 124850, 125105, 128713, 128786, and 129058 (Hungary); the Council of Science and Industrial Research, India; the HOMING PLUS program of the Foundation for Polish Science, cofinanced from European Union, Regional Development Fund, the Mobility Plus program of the Ministry of Science and Higher Education, the National Science Center (Poland), contracts Harmonia 2014/14/M/ST2/00428, Opus 2014/13/B/ST2/02543, 2014/15/B/ST2/03998, and 2015/19/B/ST2/02861, Sonata-bis 2012/07/E/ST2/01406; the National Priorities Research Program by Qatar National Research Fund; the Ministry of Science and Education, grant no. 14.W03.31.0026 (Russia); the Programa Estatal de Fomento de la Investigación Científica y Técnica de Excelencia María de Maeztu, grant MDM-2015-0509 and the Programa Severo Ochoa del Principado de Asturias; the Thalis and Aristeia programs cofinanced by EU-ESF and the Greek NSRF; the Rachadapisek Sompot Fund for Postdoctoral Fellowship, Chulalongkorn University and the Chulalongkorn Academic into Its 2nd Century Project Advancement Project (Thailand); the Kavli Foundation; the Nvidia Corporation; the SuperMicro Corporation; the Welch Foundation, contract C-1845; and the Weston Havens Foundation (USA).

References

[1] G. Cavoto et al., "A review of the intrinsic heavy quark content of the nucleon", *Advances in High Energy Physics* **2015** (2015) 231547, doi:10.1155/2015/231547, arXiv:1504.06287.

[2] T.-J. Hou et al., "Ct14 intrinsic charm parton distribution functions from cteq-tea global analysis", *Journal of High Energy Physics* **2018** (2018), no. 2, 59, doi:10.1007/JHEP02(2018)059, arXiv:1707.00657.

[3] R. D. Ball et al., "A determination of the charm content of the proton", *The European Physical Journal C* **76** (2016), no. 11, 647, doi:10.1140/epjc/s10052-016-4469-y, arXiv:1605.06515.

[4] CMS Collaboration, "Search for the pair production of third-generation squarks with two-body decays to a bottom or charm quark and a neutralino in proton-proton collisions at $\sqrt{s}$ = 13 TeV", *Phys. Lett. B* **778** (2018) 263, doi:10.1016/j.physletb.2018.01.012, arXiv:1707.07274.

[5] CMS Collaboration, "Measurement of associated Z +charm production in proton-proton collisions at $\sqrt{s} = 8$ TeV", *Eur. Phys. J. C* **78** (2018) 287, doi:10.1140/epjc/s10052-018-5752-x, arXiv:1711.02143.

[6] CMS Collaboration, "Identification of heavy-flavour jets with the CMS detector in pp collisions at 13 TeV", *JINST* **13** (2018) P05011, doi:10.1088/1748-0221/13/05/P05011, arXiv:1712.07158.

[7] CMS Collaboration, "The CMS trigger system", *JINST* **12** (2017) P01020, doi:10.1088/1748-0221/12/01/P01020, arXiv:1609.02366.

[8] CMS Collaboration, "The CMS experiment at the CERN LHC", *JINST* **3** (2008) S08004, doi:10.1088/1748-0221/3/08/S08004.

[9] J. Alwall et al., "The automated computation of tree-level and next-to-leading order differential cross sections, and their matching to parton shower simulations", *JHEP* **07** (2014) 079, doi:10.1007/JHEP07(2014)079, arXiv:1405.0301.

[10] T. Gleisberg, S. Hoeche, F. Krauss, M. Schoenherr, S. Schumann, F. Siegert, and J. Winter, "Event generation with SHERPA 1.1", *JHEP* **07** (2008) 0902, doi:10.1088/1126-6708/2009/02/007, arXiv:0811.4622.

[11] F. Buccioni, J. Lang, J.M. Lindert, P. Maierhofer, S. Pozzorini, H. Zhang, and M.F. Zoller, "OpenLoops 2", *Eur. Phys. J. C* **79** (2019) 866, doi:10.1140/epjc/s10052-019-7306-2, arXiv:1907.13071.

[12] Y. Li and F. Petriello, "Combining QCD and electroweak corrections to dilepton production in the framework of the FEWZ simulation code", *Phys. Rev. D* **86** (2012) 094034, doi:10.1103/PhysRevD.86.094034, arXiv:1208.5967.

[13] NNPDF Collaboration, "Parton distributions for the LHC run II", *JHEP* **04** (2015) 040, doi:10.1007/JHEP04(2015)040, arXiv:1410.8849.

[14] CMS Collaboration, "Measurement of the $\mathrm{t\bar{t}}$ production cross section using events with one lepton and at least one jet in pp collisions at $\sqrt{s} = 13\,\text{TeV}$", *JHEP* **09** (2017) 051, doi:10.1007/JHEP09(2017)051, arXiv:1701.06228.

[15] CMS Collaboration, "Measurement of the $\mathrm{t\bar{t}}$ production cross section using events in the $\mathrm{e}\mu$ final state in pp collisions at $\sqrt{s} = 13\,\text{TeV}$", *Eur. Phys. J. C* **77** (2017) 172, doi:10.1140/epjc/s10052-017-4718-8, arXiv:1611.04040.

[16] N. Kidonakis, "Differential and total cross sections for top pair and single top production", in *Proceedings of the XX International Workshop on Deep-Inelastic Scattering and Related Subjects*. Bonn, Germany, 2012. arXiv:1205.3453. doi:10.3204/DESY-PROC-2012-02/251.

[17] S. Alioli, P. Nason, C. Oleari, and E. Re, "NLO single-top production matched with shower in POWHEG: s- and t-channel contributions", *JHEP* **09** (2009) 111, doi:10.1088/1126-6708/2009/09/111, arXiv:0907.4076. [Erratum: doi:10.1007/JHEP02(2010)011].

[18] P. Nason, "A new method for combining NLO QCD with shower Monte Carlo algorithms", *JHEP* **11** (2004) 040, doi:10.1088/1126-6708/2004/11/040, arXiv:hep-ph/0409146.

[19] S. Frixione, P. Nason, and C. Oleari, "Matching NLO QCD computations with parton shower simulations: the POWHEG method", *JHEP* **11** (2007) 070, doi:10.1088/1126-6708/2007/11/070, arXiv:0709.2092.

[20] S. Alioli, P. Nason, C. Oleari, and E. Re, "A general framework for implementing NLO calculations in shower Monte Carlo programs: the POWHEG BOX", *JHEP* **06** (2010) 043, doi:10.1007/JHEP06(2010)043, arXiv:1002.2581.

[21] T. Sjöstrand et al., "An introduction to PYTHIA 8.2", *Comput. Phys. Commun.* **191** (2015) 159, doi:10.1016/j.cpc.2015.01.024, arXiv:1410.3012.

[22] CMS Collaboration, "Event generator tunes obtained from underlying event and multiparton scattering measurements", *Eur. Phys. J. C* **76** (2016) 155, doi:10.1140/epjc/s10052-016-3988-x, arXiv:1512.00815.

[23] CMS Collaboration, "Investigations of the impact of the parton shower tuning in PYTHIA8 in the modelling of $\mathrm{t\bar{t}}$ at $\sqrt{s} = 8$ and 13 TeV", CMS Physics Analysis Summary CMS-PAS-TOP-16-021, 2016.

[24] R. D. Ball et al., "Parton distributions with LHC data", *Nucl. Phys. B* **867** (2013) 244, doi:10.1016/j.nuclphysb.2012.10.003, arXiv:1207.1303.

[25] J. Alwall et al., "Comparative study of various algorithms for the merging of parton showers and matrix elements in hadronic collisions", *Eur. Phys. J. C* **53** (2008) 473, doi:10.1140/epjc/s10052-007-0490-5, arXiv:0706.2569.

[26] J. Alwall, S. de Visscher, and F. Maltoni, "QCD radiation in the production of heavy colored particles at the LHC", *JHEP* **02** (2009) 017, doi:10.1088/1126-6708/2009/02/017, arXiv:0810.5350.

[27] R. Frederix and S. Frixione, "Merging meets matching in MC@NLO", *JHEP* **12** (2012) 061, doi:10.1007/JHEP12(2012)061, arXiv:1209.6215.

[28] GEANT4 Collaboration, "GEANT4 — a simulation toolkit", *Nucl. Instrum. Meth. A* **506** (2003) 250, doi:10.1016/S0168-9002(03)01368-8.

[29] CMS Collaboration, "Particle-flow reconstruction and global event description with the CMS detector", *JINST* **12** (2017) P10003, doi:10.1088/1748-0221/12/10/P10003, arXiv:1706.04965.

[30] CMS Collaboration, "Performance of electron reconstruction and selection with the CMS detector in proton-proton collisions at $\sqrt{s} = 8$ TeV", *JINST* **10** (2015) P06005, doi:10.1088/1748-0221/10/06/P06005, arXiv:1502.02701.

[31] CMS Collaboration, "Performance of the CMS muon detector and muon reconstruction with proton-proton collisions at $\sqrt{s} = 13$ TeV", *JINST* **13** (2018) P06015, doi:10.1088/1748-0221/13/06/P06015, arXiv:1804.04528.

[32] M. Cacciari and G. P. Salam, "Pileup subtraction using jet areas", *Phys. Lett. B* **659** (2008) 119, doi:10.1016/j.physletb.2007.09.077, arXiv:0707.1378.

[33] M. Cacciari, G. P. Salam, and G. Soyez, "The anti-k_{T} jet clustering algorithm", *JHEP* **04** (2008) 063, doi:10.1088/1126-6708/2008/04/063, arXiv:0802.1189.

[34] M. Cacciari, G. P. Salam, and G. Soyez, "FastJet user manual", *Eur. Phys. J. C* **72** (2012) 1896, doi:10.1140/epjc/s10052-012-1896-2, arXiv:1111.6097.

[35] M. Cacciari and G. P. Salam, "Pileup subtraction using jet areas", *Phys. Lett. B* **659** (2008) 119, doi:10.1016/j.physletb.2007.09.077, arXiv:0707.1378.

[36] CMS Collaboration, "Jet energy scale and resolution in the CMS experiment in pp collisions at 8 TeV", *JINST* **12** (2017) P02014, doi:10.1088/1748-0221/12/02/P02014, arXiv:1607.03663.

[37] CMS Collaboration, "Performance of missing transverse momentum in proton-proton collisions at $\sqrt{s} = 13$ TeV using the CMS detector", *JINST* **14** (2019) P07004, doi:10.1088/1748-0221/14/07/P07004, arXiv:1903.06078.

[38] CMS Collaboration, "Pileup mitigation at CMS in 13 TeV data", *Journal of Instrumentation* **15** (2020), no. 09, P09018–P09018, doi:10.1088/1748-0221/15/09/p09018, arXiv:2003.00503.

[39] CMS Collaboration, "Measurement of the inclusive W and Z production cross sections in pp collisions at $\sqrt{s} = 7$ TeV with the CMS experiment", *JHEP* **10** (2011) 132, doi:10.1007/JHEP10(2011)132, arXiv:1107.4789.

[40] CMS Collaboration, "Measurement of $B\bar{B}$ angular correlations based on secondary vertex reconstruction at $\sqrt{s} = 7$ TeV", *JHEP* **03** (2011) 136, doi:10.1007/JHEP03(2011)136, arXiv:1102.3194.

[41] S. Schmitt, "TUnfold: an algorithm for correcting migration effects in high energy physics", *JINST* **7** (2012) T10003, doi:10.1088/1748-0221/7/10/T10003, arXiv:1205.6201.

[42] CMS Collaboration, "Measurement of the inelastic proton-proton cross section at $\sqrt{s} = 13$ TeV", *JHEP* **07** (2018) 161, doi:10.1007/JHEP07(2018)161, arXiv:1802.02613.

[43] M. Czakon, P. Fiedler, and A. Mitov, "Total top quark pair production cross section at hadron colliders through $O(\alpha_S^4)$", *Phys. Rev. Lett.* **110** (2013) 252004, doi:10.1103/PhysRevLett.110.252004, arXiv:1303.6254.

[44] CMS Collaboration, "CMS Luminosity Measurements for the 2016 Data Taking Period", Technical Report CMS-PAS-LUM-17-001, CERN, Geneva, 2017.

[45] J. Kieseler, "A method and tool for combining differential or inclusive measurements obtained with simultaneously constrained uncertainties", *Eur. Phys. J. C* **77** (2017) 792, doi:10.1140/epjc/s10052-017-5345-0, arXiv:1706.01681.

[46] CMS Collaboration, "Measurement of differential cross sections for z boson production in association with jets in proton-proton collisions at $\sqrt{s} = 8$ TeV", *The European Physical Journal C* **78** (2018), no. 11, 965, doi:10.1140/epjc/s10052-018-6373-0, arXiv:1804.05252.

A Post-fit secondary vertex mass distributions

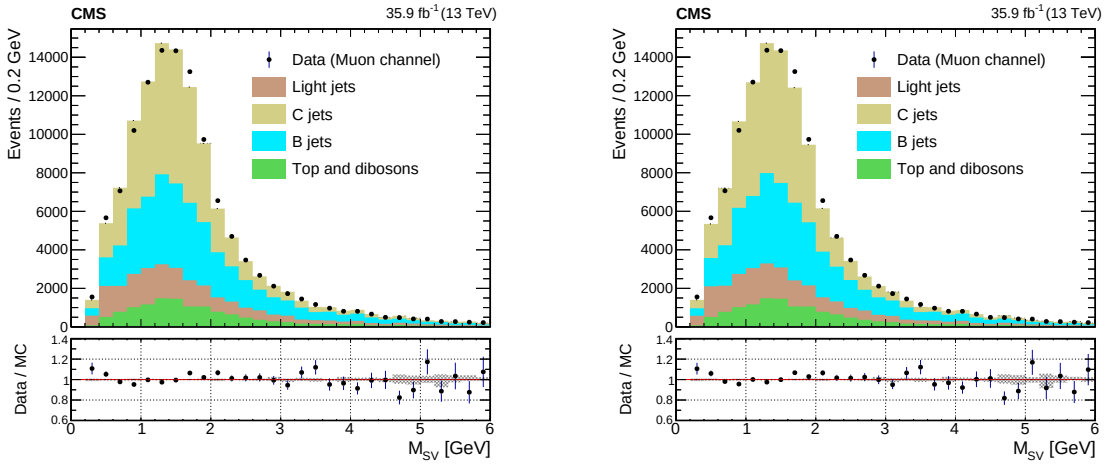

Figure 7: Distribution of the secondary vertex mass of the highest-p_T c-tagged central jet, for electron channel.The observed data is compared to the different signal and background components in simulation, after normalization scale factors as function of Z p_T (left) and c-tagged central jet p_T (right) are applied.

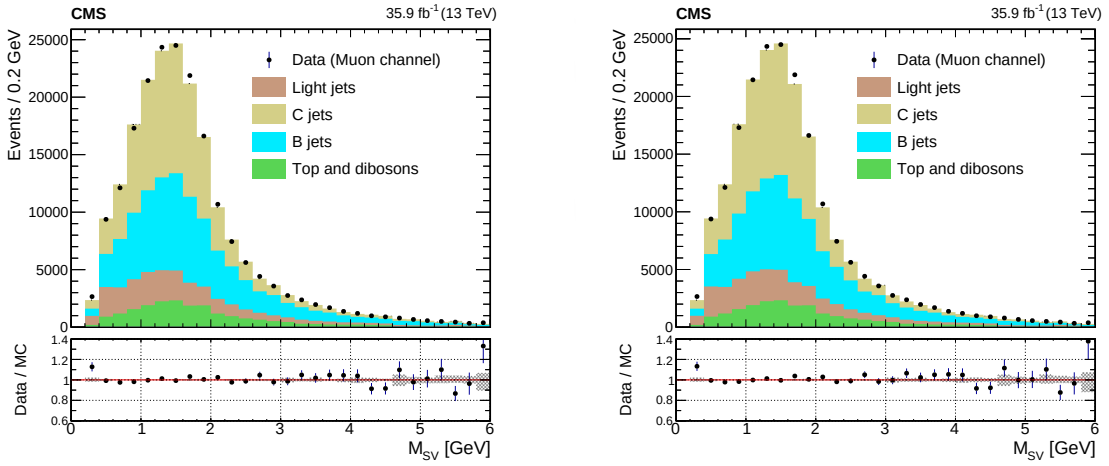

Figure 8: Distribution of the secondary vertex mass of the highest-p_T c-tagged central jet, for muon channel.The observed data is compared to the different signal and background components in simulation, after normalization scale factors as function of Z p_T (left) and c-tagged central jet p_T (right) are applied.